Midplane measurements of MeV ion confinement in TFTR

R. Boivin, S. Kilpatrick, D. Manos, and S. Zweben
Princeton Plasma Physics Laboratory, P.O. Box 451, Princeton, New Jersey 08543

(Presented on 9 May 1990)

A new detector has been designed and installed on TFTR for studying the confinement of MeV ions, especially for measuring the losses due to the toroidal field ripple. It is located just below the outer midplane where the peak in ripple-induced losses is expected. The detector consists of a scintillator [ZnS(Ag)] and collimating apertures mounted on a radially movable probe. New design features of this detector are presented along with some of the first results.

I. INTRODUCTION

Previous measurements on TFTR of losses to the wall of alpha-like fusion product ions showed that (in the absence of MHD activity) their confinement followed neoclassical calculations.[1] These measurements were restricted to the bottom portion of the vessel, i.e., poloidally between $-45°$ and $-90°$ from the outer midplane.

Recent developments in the theory of toroidal magnetic field ripple diffusion have shown that the TF ripple-induced losses should be highly localized just below the outer midplane.[2] Such losses can potentially cause problems associated with heat loads on the first wall, for example, in ITER.[3] The effect of TF ripple can be seen in Fig. 1, where a 1 MeV triton orbit is shown. Particles whose banana tips lie in the stochastic region[4] (shaded area in the figure) would wander out and eventually hit the wall below the midplane. Also shown is the approximate position of the new detector, located where the maximum in ripple-induced losses is expected (between $-10°$ and $-20°$).

This new detector, recently installed on TFTR, is mounted on a radially movable probe and uses the same scintillation technique described in Ref. 1. It is located near the outer midplane and has the ability to move inside the radius of the TFTR limiters (while still outside the plasma). This radial movement gives the detector the new capability of sampling confined ions, thus allowing a direct comparison between confined and lost MeV ion populations. The two main difficulties encountered during the design were related to the optical coupling between the scintillator and the camera, and to the thermal insulation of the internal parts. These new aspects are discussed in Sec. II, while the first results are described in Sec. III.

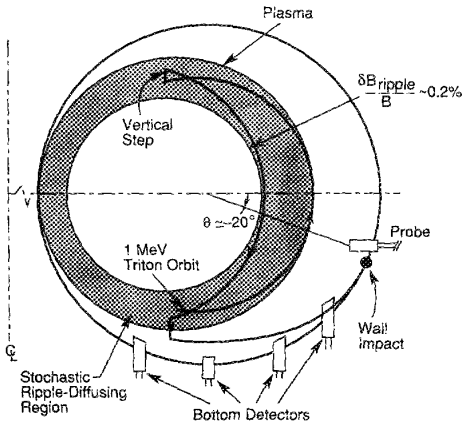

FIG. 1. Poloidal cross section of TFTR. Shown is a 1 MeV triton ripple-diffusing out and hitting the wall below the outer midplane.

II. DESIGN

The mechanical design of the detector and its probe support is shown in Fig. 2. The probe is installed behind a Torus isolation valve which permits easy removal without the need of a machine opening. With an overall dimension of approximately 3 m, the probe has a stroke of 109 cm, of which 27 are inside the first wall of the torus. The first 10 cm inside the torus lie in the shadow of the "RF" limiters (approximately 90° and 145° away in the co-direction). This probe is located at 35.6 cm below the midplane at the same toroidal angle as the bottom detectors mentioned above.

A. Detection system

In the probe head, at the extreme left on the diagram, we have the set of collimating apertures and the scintillator. They are very similar in design to the ones used in the other detectors, and are described more extensively in Refs. 1 and 5. The apertures are dimensioned and positioned for measuring the ion flux in the range 40°–80° in pitch angle and between 4 and 10 cm in gyroradius. The presence of a 3 μm aluminum foil stops the 0.8 MeV ^{3}He but let the tritons (>0.6 MeV), the protons (>0.4 MeV), and the alphas (>1.2 MeV) pass. Work is under way to measure the relative contributions of the 1 MeV tritons and 3 MeV protons to the light signal emitted by the scintillator. Tritons are believed to account for approximately 70% of the total light output.

B. Protection and support

A nonmagnetic, light-tight, 0.64-cm-thick stainless-steel box is used to support the scintillator, apertures, and other internal parts and to prevent x rays from reaching the scintillator. The stainless-steel box is protected from the plasma heat flux by a cylindrical 4-D weave carbon/carbon composite[6] armor 1 cm thick. To minimize the heat conduction the two are not in direct contact except at the supporting ring at the back of the probe head. Two thermocouples, one inside the box, near the scintillator, and

 0034-6748/90/103208-03$02.00

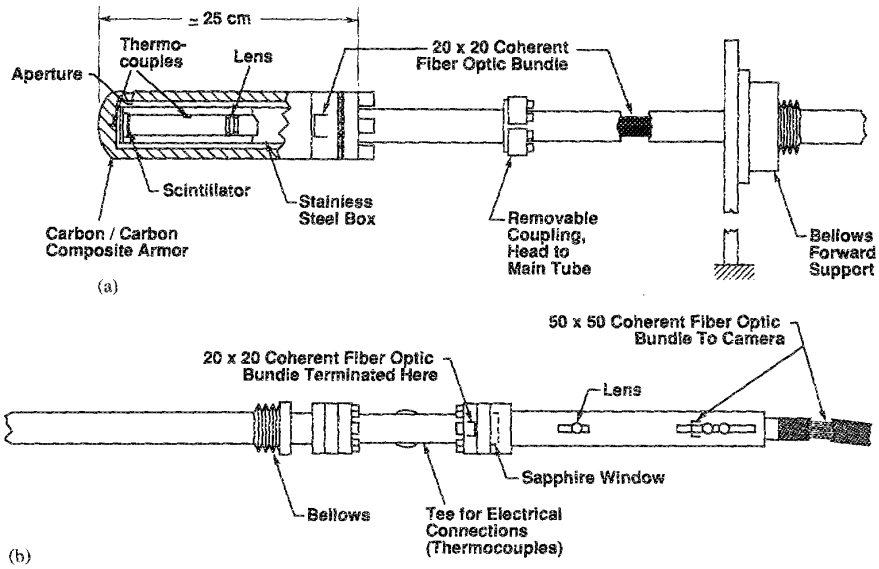

FIG. 2. Layout of the midplane detector and its probe support. Particles penetrate through the aperture at the left and hit the scintillator. Fiber optics transmit the light through the probe shaft to an external fiber bundle leading to the camera.

the other one outside the box, implanted in the tip of the armor, are used to monitor the temperature of the probe head. On the bench the scintillator light emission was found to be reduced above about 150 °C, although the scintillator could reach >300 °C without permanent damage.

C. Light transmission

For such a long and narrow probe it was necessary to use fiber optics to transmit light from the scintillator to the vacuum window. The coherent fiber optic bundle is made of a 20×20 array of 450 μm quartz fibers, approximately 2.1 m long, and is terminated by two stainless-steel ferrules. The number of fibers was chosen to be the minimum consistent with the spatial resolution set by the aperture geometry. The only drawback of quartz fibers is their relatively small acceptance angle (25.4° full angle) which limits the amount of light one can collect from the scintillator. A 2.2 cm quartz lens (with a 3.2 cm focal length) cut square is used to image and magnify (by a factor of 2.3) the scintillator image onto the bundle.

At the other end of the probe, shown in Fig. 2(b) are the relay components between the in-vacuum bundle and the external bundle. The 20×20 bundle is terminated next to a 1.6-cm-diam sapphire window, and a 2.54-cm-diam quartz lens (with a 3.8 cm focal length) relays the scintillator image between the two bundles and demagnifies it by a factor of 0.75. From there a 20 m coherent fiber optic bundle, made of a 50×50 array of 250 μm quartz fibers, carries the light to the remotely located camera and photomultiplier tubes.

With the probe fully assembled on the bench, a uniform and lambertian blue source of light (made of a halogen lamp, a white diffuser, and a blue filter @450 nm, the scintillator emission wavelength) was put at the scintillator location. The optical efficiency of the detector was measured in comparing the light intensity at the source and at the end of the 50×50 fiber bundle using a fiber optic coupled to a photomultiplier tube. For a given point on the scintillator, not too close to the edges, the detector was found to transmit 6.3% of the total light emitted. A relative calibration between the different detectors was performed and showed that optical coupling for this midplane detector is 4 to 10 times less efficient than that of the other detectors.

The aperture dimensions were chosen, in this first iteration, to be identical to the bottom detector aperture. The finite dimensions of the apertures are the principal limits to the pitch angle and the energy resolution. An extensive discussion about the resolution capabilities in this type of detector can be found in Ref. 7. In our case the pitch angle resolution is approximately $\pm8°$ whereas the energy resolution is no better than $\pm100\%$. The optical contribution to the resolution was checked using a test pattern put at the scintillator location. A picture of the image taken at the end of the 50×50 fiber bundle can be seen in Fig. 3.

III. RESULTS

The first results were obtained in January 1990. For the probe in the shadow of the "RF" limiters the light

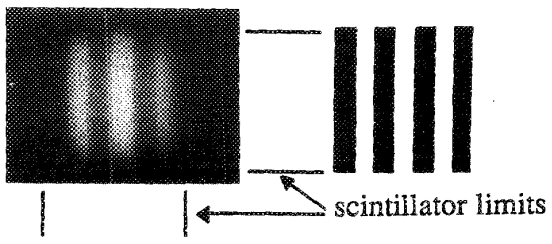

FIG. 3. Bench test picture (left) of the optical resolution of the detector using a test pattern (right) put at the scintillator location. The vignetting effect (dark corners) is clearly visible.

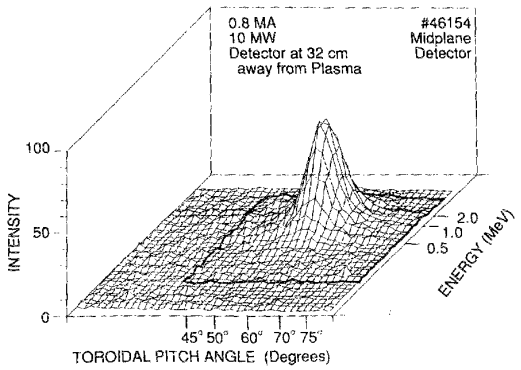

FIG. 4. 3-D plot of a typical light signal from the scintillator. Shown is the light intensity, integrated over a shot, as a function of the toroidal pitch angle and energy of the incident particles.

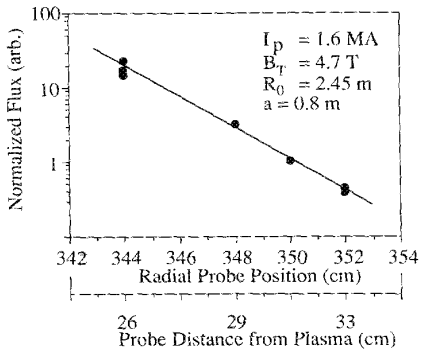

FIG. 5. Ion flux, normalized by the neutron source strength, as a function of the radial position of the probe. The "RF" limiter radius is located at $R = 353$ cm.

signal from tritons and protons was found to be similar to the other detectors. At this location, the probe generally handled heat loads quite well (increase typically less than 3 °C per shot), an exception being with large major radius plasmas, with high power or at high shot repetition rate (< 10 min between shots) when the probe needed to be retracted temporarily after ~ 15 shots (the increase being around 5 °C per shot).

Figure 4 shows a 3-D plot (with $P_{\mathrm{NBI}} \sim 10$ MW, $I_p = 0.8$ MA, $B_T = 4.7$ T, $R = 2.45$ m, and $a = 0.8$ m) of the image of the scintillator viewed by the camera. The light intensity is plotted as a function of toroidal pitch angle (x axis) and energy for tritons (or gyroradius, y axis). The peak in flux occurs at a pitch angle of approximately 60° and energy of 1 MeV for the tritons (or equivalently 3 MeV for the protons), which is approximately consistent, in this case, with first-orbit loss calculations. The background, mainly neutron and gamma scintillation in the quartz fiber optic bundles, is usually small, typically less than 15% and can be partially removed using a blue filter located in front of the camera.

The first measurements of the radial dependence of the MeV ion flux are shown in Fig. 5. The pitch angle and energy integrated ion flux at its peak in time is plotted, normalized by the neutron source strength, as a function of the probe position (different shots, with plasma conditions described above but with $I_p = 1.6$ MA). The flux increases as the probe moves in, either sampling confined ions or particles slowly diffusing out (as in ripple-induced diffusion).

IV. FUTURE WORK

Theoretical work is needed to help distinguish the ripple losses from the prompt losses (which are always present) and to model the measurements of confined ions seen during the probe radial scan. An absolute calibration of the detector is also in progress, and should enable us to absolutely calibrate the MeV ion flux to the detectors.

Future plans also include the study of ion losses due to superbanana ripple trapping, which occur at pitch angles of $90° \pm 10°$ (and so are not observable by any detector at this moment). The present detector is also being used to study the confinement of the energetic hydrogen tail ions generated by ICRF minority heating.

ACKNOWLEDGMENTS

We would like to thank K. Young, L. Johnson, and J. Strachan for supporting this new diagnostic and T. Bennett, T. Deverell, M. Diesso, S. Hayes, J. Montague, D. Palladino, and B. Parsells for their help in building it.

[1] S. J. Zweben, Nucl. Fusion **29**, 825 (1989).
[2] Y. I. Kolesnichenko and V. A. Yavorskij, Nucl. Fusion **29**, 1319 (1989).
[3] Y. I. Kolesnichenko and D. J. Sigmar, Nucl. Fusion **30**, 777 (1990).
[4] R. B. White and H. E. Mynick, Phys. Fluids B **1**, 980 (1989).
[5] S. J. Zweben, Rev. Sci. Instrum. **57**, 1774 (1986).
[6] Fiber Materials Inc., Biddeford, ME 04005.
[7] S. J. Zweben, PPPL report No. 2686 Nucl. Fus.(to be published).